# Fabrication of Highly Stable Cs3Cu2I5-in-Glass Composite for X-Ray Imaging by SPS Technique

Panyi Wang, Mengmeng Meng, Man Nie, Xiaoyu Hu, Peiqing Cai, Muzhi Cai, Lei Lei, Laurent Calvez, Xianghua Zhang, Shiqing Xu

**Fabrication of Highly Stable $Cs_3Cu_2I_5$-in-Glass Composite for X-ray Imaging by SPS Technique**

*Panyi Wang, Mengmeng Meng, Man Nie, Xiaoyu Hu, Peiqing Cai, Muzhi Cai *, Lei Lei *, Laurent Calvez, Xianghua Zhang, and Shiqing Xu*

P. Wang, M. Meng, M. Nie, X. Hu, P. Cai, M. Cai, L. Lei, S. Xu
Key Laboratory of Rare Earth Optoelectronic Materials and Devices of Zhejiang Province, Institute of Optoelectronic Materials and Devices, China Jiliang University, Hangzhou 310018, China
E-mail: caimuzhi@cjlu.edu.cn; leilei@cjlu.edu.cn

P. Wang, L. Calvez, X. Zhang
ISCR (Institut des Sciences Chimiques de Rennes) UMR 6226, Univ Rennes, CNRS, F35000 Rennes, France

The development of all-inorganic lead-free $Cs_3Cu_2I_5$ perovskite materials has garnered significant attention due to their non-toxic nature and unique optoelectronic properties, especially in the field of X-ray detection. However, the stability of perovskites remains a major concern for their optical applications. In this study, highly stable $Cs_3Cu_2I_5$-in-glass composite ($Cs_3Cu_2I_5$@Borosilicate) was fabricated by spark plasma sintering (SPS), a rapid and low-temperature sintering process. The $Cs_3Cu_2I_5$@Borosilicate composite exhibits strong photoluminescence even after prolonged immersion in various polar solvents, whereas $Cs_3Cu_2I_5$ perovskite loses its photoluminescence within seconds. Moreover, the $Cs_3Cu_2I_5$@Borosilicate composite demonstrates robust radio-luminescence under X-ray irradiation, and its potential as a scintillator material is validated through prototype X-ray imaging with high spatial resolution (~7 lp $mm^{-1}$). This innovative composite material holds immense potential for scintillation applications and represents a promising approach for encapsulating perovskites in a transparent amorphous medium.

Keywords: lead-free perovskite; $Cs_3Cu_2I_5$ composite; scintillator; X-ray imaging

## 1. Introduction

Metal halide perovskites (MHPs) have attracted wide attention in light-emission diodes (LEDs),[1] photovoltaics,[2] lasers,[3] polarized light electronic devices[4] and other optoelectronic applications owing to their high photoluminescence quantum yield (PLQY), tunable bandgap and efficient electroluminescence.[5] Notably, MHPs have emerged as new potential materials in scintillator-based radiation detection due to high effective atomic number ($Z_{eff}$), strong and tunable radioluminescence (RL), fast scintillation response and high-resolution X-ray imaging.[6] Recently, all-inorganic ternary copper lead-free halide perovskite, $Cs_3Cu_2I_5$, has gained attention for its high PLQY and light yield (LY), environment-friendly and large Stokes shifts.[7] These perovskites have shown potential in scientific research and practical applications such as radiation detection,[8] X-ray imaging[9] and nuclear batteries.[10] However, the low formation enthalpy of perovskites makes them prone to damage, as they can be easily formed or decomposed under certain conditions.[11] These factors limit their practical applications and call for further research and optimization efforts.

Various strategies have been proposed to address these challenges faced by MHPs, among which inorganic glass matrix encapsulation is considered to be an effective method to improve thermal and chemical stability.[12] Inorganic glass is an excellent medium for optical application in society, industry, and scientific research, mainly due to its unequaled optical transparency, various efficient sensitized ions can be doped as well as prominent mechanical, chemical, and thermal resistance.[13] Currently, two main strategies are used to fabricate MHPs composite glass: the “top-down” and “bottom-up” approaches.[14] However, to the best of our knowledge, very few studies have reported on $Cs_3Cu_2I_5$ composite glass due to the low crystallinity of the in-situ crystallization method, which is the main technique for obtaining MHPs composite glass using a top-down strategy.[15] The main technique using a bottom-up strategy is sintering or melting mixtures of inorganic glass and MHPs. However, conventional pressure or pressureless sintering methods require long heating, sintering and cooling processes, which can damage the structure of the MHPs.[16] Recently, we reported that multicomponent glasses can be reproduced near their glass transition temperature using spark plasma sintering (SPS), and organic molecules with low degradation temperatures have been successfully embedded in an inorganic glass matrix.[17] Therefore, embedding MHPs in an inorganic glass matrix is possible, but has rarely been reported.

In this work, the $Cs_3Cu_2I_5$-in-glass composite was prepared by a bottom-up strategy. By employing SPS of crystalline $Cs_3Cu_2I_5$ and various soft glass matrices, we were able to fabricate $Cs_3Cu_2I_5$-in-glass composites with different particle loading ratios. It is noteworthy that

$Cs_3Cu_2I_5$ MHPs and inorganic glasses, despite their distinct chemical compositions, can be processed using industrial MHP processes to create high-performance composites. Given the $Cs_3Cu_2I_5$ MHPs' potential as scintillator materials, the glass matrix must be suitable for scintillator applications. Therefore, we selected borosilicate glass as the encapsulation glass matrix due to its exceptional mechanical and chemical properties. The $Cs_3Cu_2I_5$-in-glass composites maintain the superb optical properties of the $Cs_3Cu_2I_5$ MHPs and exhibit exceptional stability de to the advantages of the SPS technology as well as the protection and capping effects provided by the glass matrix.[18] These findings suggest that the $Cs_3Cu_2I_5$@Borosilicate scintillator enables high-resolution X-ray imaging with remarkable stability, even in moist environments, under X-ray illumination.

## 2. Results and Discussion

$Cs_3Cu_2I_5$ MHPs were synthesized using an anti-solvent method, resulting in particles ranging from nanometers to microns, as confirmed in Figure S1. Energy dispersive X-ray spectroscopy (EDS) analysis revealed an average atomic ratio of Cs, Cu, and I in $Cs_3Cu_2I_5$ of 3.06 : 2 : 4.83, which aligns closely with the stoichiometric results (Figure S2 and Table S1). X-ray diffraction (XRD) confirmed the structure of the synthesized $Cs_3Cu_2I_5$ MHP, which closely matched the orthorhombic $Cs_3Cu_2I_5$ structure (PDF#01-072-9850), as shown in **Figure 1**a. Earlier studies have reported that $Cs_3Cu_2I_5$ chemically decomposed to $CsCu_2I_3$ under high-temperature and polar solvent induction (Figure S3).[19] Consequently, embedding $Cs_3Cu_2I_5$ into inorganic glass ensures both chemical and thermal stability, thereby enabling the possibility of long-term operation of equipment in extreme environments and broadening its application scope in optical and scintillation fields.[13]

To ensure successful embedding of the $Cs_3Cu_2I_5$ MHPs into the glass matrix, an investigation into the thermal stability of the $Cs_3Cu_2I_5$ MHPs was conducted. The thermogravimetric analysis (TGA) and differential scanning calorimetry (DSC) measurements were conducted in a nitrogen atmosphere. As shown in Figure 1b, the melting point of the $Cs_3Cu_2I_5$ MHPs is 662 K, and the thermal event observed at 623K may be caused by a eutectic reaction occurring between residual traces of CsI and $Cs_3Cu_2I_5$ MHPs.[20] The TGA results present that the weight loss of $Cs_3Cu_2I_5$ MHPs was negligible in the range of 303 K to 771 K, indicating that the $Cs_3Cu_2I_5$ MHPs show good thermal stability in nitrogen atmosphere. In addition, the structural evolution of $Cs_3Cu_2I_5$ MHPs in a vacuum was further investigated using in-situ XRD. The $Cs_3Cu_2I_5$ MHPs were heated from RT to 643 K, as shown in Figure S4. As the temperature increases, the lattice expands and the diffraction peak shifts to a lower angle,

consistent with previous reports.[21] Through in-situ XRD observation, it was found that the crystal structure of $Cs_3Cu_2I_5$ MHPs remains stable at various temperatures. Overall, $Cs_3Cu_2I_5$ MHP exhibits good thermal stability in an inert atmosphere, there is a large processing temperature window for embedding it into the glass matrix.

Based on the thermal properties of $Cs_3Cu_2I_5$ MHPs, borosilicate glass was chosen as the matrix material. Borosilicate glass has a suitable glass transition temperature, good mechanical properties, and stable chemical properties. The thermal properties of the borosilicate glass are shown in Figure 1c, and the glass transition temperature ($T_g$) is estimated to be 660 K. A series of borosilicate glasses embedded with $Cs_3Cu_2I_5$ MHPs were rapidly fabricated at 598 K under vacuum condition using SPS, with the manufacturing process depicted in Figure 1d. Compared with other sintering methods, SPS technology has multiple advantages for the preparation of composite glass, including fast heating speed, low sintering temperature, vacuum sintering, and short overall production time, which ensure the preservation of the functional materials against potential damage throughout the fabrication process.[17, 22] The optimal sintering parameters that do not require powder preforming or prolonged heat treatment are displayed in Figure 1e. The temperature applied to the borosilicate pellets increased from room temperature (RT) to 598 K within 5 minutes, with a maximum heating rate of 80 K $min^{-1}$. The applied pressure gradually increased from 8.7 MPa to 18.7 MPa. The composite glass can be produced after 3 minutes of insulation and pressure retention, noted as $Cs_3Cu_2I_5$@Borosilicate. Hence, the preparation of composite glass using SPS technology holds significant promise and potential.

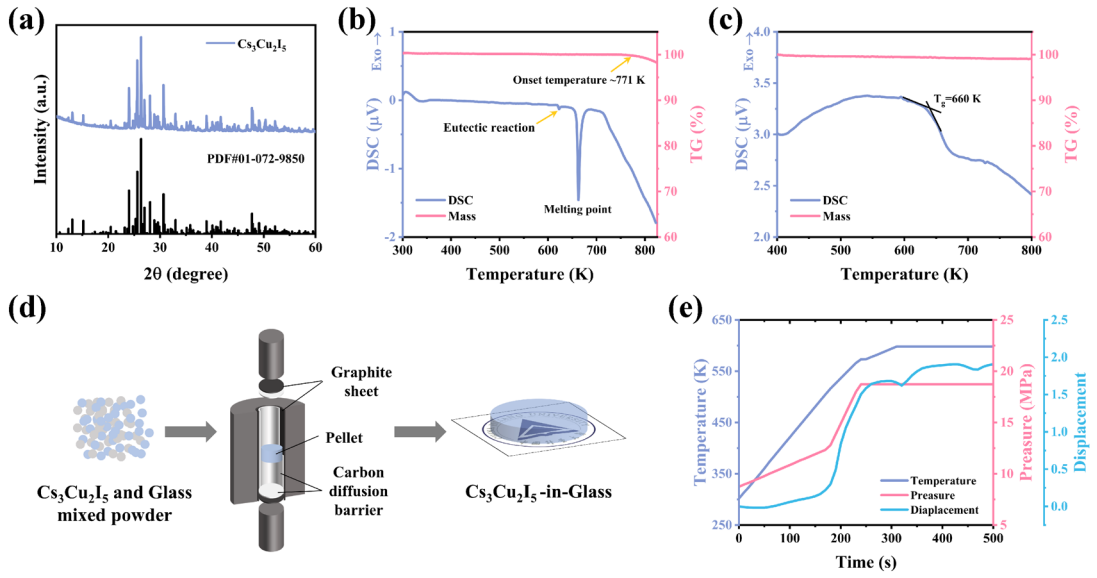


**Figure 1.** a) XRD patterns of $Cs_3Cu_2I_5$ MHPs. TG-DSC of b) $Cs_3Cu_2I_5$ MHPs and c) borosilicate glass matrix. d) Schematic illustration for the synthesis of $Cs_3Cu_2I_5$ embedded into borosilicate glass composites. e) SPS sintering parameters.

The photophysical properties of the $Cs_3Cu_2I_5$@Borosilicate composite were examined. Both the $Cs_3Cu_2I_5$ MHPs and $Cs_3Cu_2I_5$@Borosilicate composite exhibited a photoluminescence (PL) peak at approximately 445 nm, while the photoluminescence excitation spectrum (PLE) peak occurred at 305 nm, indicating a significant Stokes shift, as shown in **Figure 2**a. Figure S5 displays the PL decay of the $Cs_3Cu_2I_5$@Borosilicate composite and $Cs_3Cu_2I_5$ MHPs measured using excitation from a 280 nm pulse laser at room temperature. The corresponding decay curves were well fitted by a single exponential function and suggested an average lifetime of 966.1 ns ($Cs_3Cu_2I_5$@Borosilicate) and 1086.7 ns ($Cs_3Cu_2I_5$ MHPs), respectively. Previous research has established that such broadband, large Stokes shift and long lifetime emission mechanism of $Cs_3Cu_2I_5$ MHPs are dominated by self-trapped excitons (STEs).[23] The exciton self-trapping processes for $Cs_3Cu_2I_5$ MHPs can be depicted in the coordinate diagram, as shown in Figure 2b.[24] The PL intensity of the $Cs_3Cu_2I_5$@Borosilicate composite increased with the concentration of $Cs_3Cu_2I_5$ MHPs, as shown in Figure 2c. The photograph in the inset of Figure 2c displays the $Cs_3Cu_2I_5$@Borosilicate emitting bright blue light under UV lamp irradiation. These results indicate that $Cs_3Cu_2I_5$@borosilicate composite exhibits similar optical properties to $Cs_3Cu_2I_5$ MHPs. The XRD patterns of a series of $Cs_3Cu_2I_5$@Borosilicate composites with different $Cs_3Cu_2I_5$ MHP concentrations are presented in Figure 2d. An amorphous hump was observed due to the as-sintered host glass, which obscures the diffraction peaks of $Cs_3Cu_2I_5$ MHPs.[25] The prominent diffraction peak at angles of 26.3° corresponding to the (222) lattice plane becomes more apparent as the content of $Cs_3Cu_2I_5$ MHPs increases, indicating that the $Cs_3Cu_2I_5$ MHPs have successfully incorporated into the glass matrix.

The scanning electron microscopy (SEM), EDS and high-resolution transmission electron microscopy (HRTEM) were used to characterize the micro-morphology of the $Cs_3Cu_2I_5$@Borosilicate composite, as shown in Figure 2e and S6. The HRTEM image shows clear lattice fringes, and the lattice spacing of $Cs_3Cu_2I_5$@Borosilicate is 0.216 nm, corresponding to the (206) planes of $Cs_3Cu_2I_5$ MHPs, as shown in the inset of Figure 2e. Scanning electron microscopy-cathodoluminescence (SEM-CL) can better explore the distribution of $Cs_3Cu_2I_5$ MHP in borosilicate glass. Clear white dots observed in CL mappings are $Cs_3Cu_2I_5$ MHP that enable us to distinguish perovskite from glass substrates (Figure 2f). The surface luminescence distribution image and CL spectra of $Cs_3Cu_2I_5$@Borosilicate are shown in Figure 2g and 2h, respectively. Points 1 and 2 show different emission spectra, which are distinguished by blue and dark, respectively. Point 1 shows a strong emission band detected at 445 nm, which is attributed to the $Cs_3Cu_2I_5$ MHP. However, for point 2, it is difficult to detect

the intensity of emission, therefore, it must belong to the host glass. These findings provide strong evidence for the stability of the $Cs_3Cu_2I_5$ MHPs within the glass matrix. Therefore, it is expected that the optical properties of the $Cs_3Cu_2I_5$ MHPs will be fully maintained within the glass matrix.

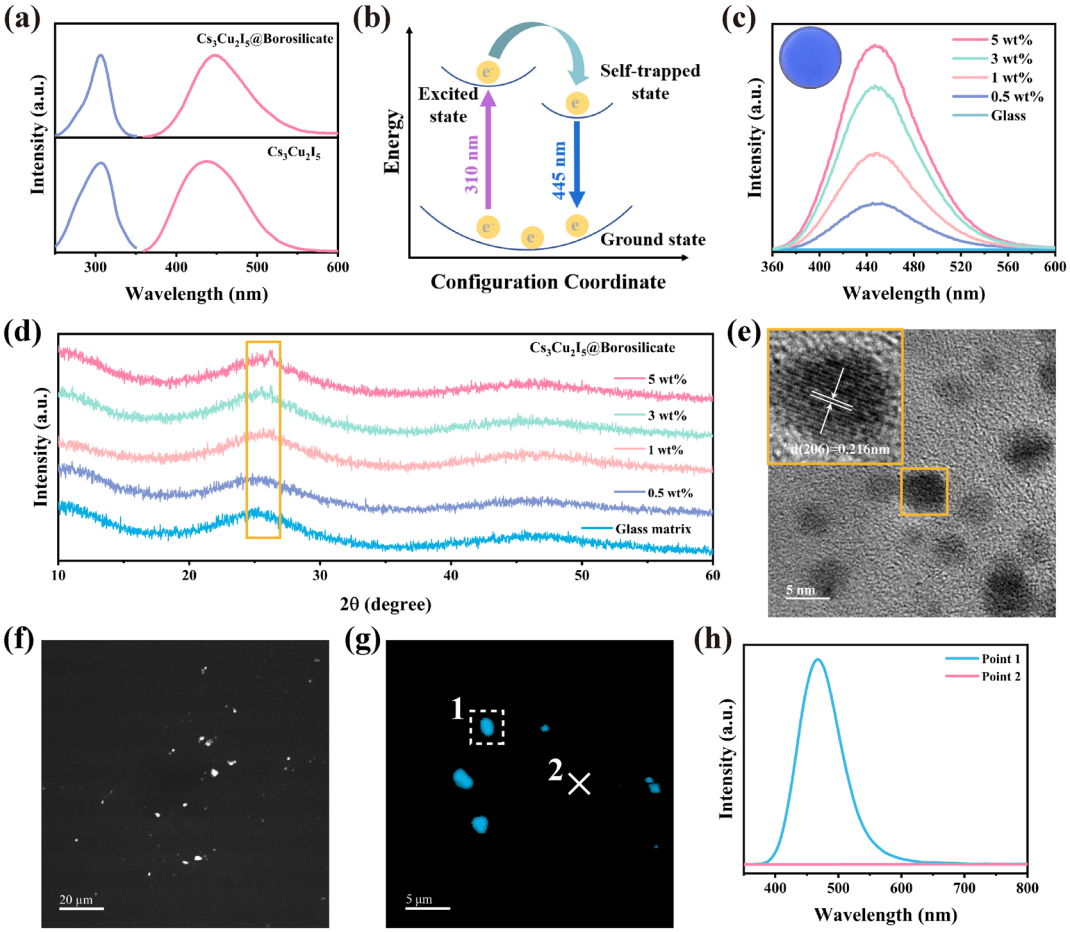


**Figure 2.** a) The photoluminescence spectra of the $Cs_3Cu_2I_5$@Borosilicate and $Cs_3Cu_2I_5$ MHPs. b) Configuration coordinate diagram for the formation mechanism of STE state in the $Cs_3Cu_2I_5$ MHP. c) The photoluminescence spectra of the $Cs_3Cu_2I_5$@Borosilicate with different $Cs_3Cu_2I_5$ content excited by 310 nm monochromatic light (the inset presents its photograph). d) XRD patterns of $Cs_3Cu_2I_5$@Borosilicate composites with different $Cs_3Cu_2I_5$ contents. e) HRTEM image of $Cs_3Cu_2I_5$@Borosilicate. f) SEM-CL image of $Cs_3Cu_2I_5$@Borosilicate. g) Partial magnification of CL spectrum of the $Cs_3Cu_2I_5$@Borosilicate. h) The point CL spectra of different single particles and glass corresponding to points from the marked area in (g).

Although $Cs_3Cu_2I_5$ MHP shows greater stability than traditional lead-based MHPs, its durability is still a challenge due to its similar ionic properties to traditional perovskites.[26] When $Cs_3Cu_2I_5$ MHPs encounter polar solvents, for example, water, chemical reaction

processes may occur $Cs_3Cu_2I_5 \rightarrow 2CsI + CsCu_2I_3$,[27] as shown in **Figure 3**a. The PL spectra of $Cs_3Cu_2I_5$ MHPs suggest their structural stability, so the PL spectra of $Cs_3Cu_2I_5$ MHPs and $Cs_3Cu_2I_5$@Borosilicate in a variety of polar solvents were investigated, as illustrated in Figure 3b and 3c. As shown in Figure 3b, when $Cs_3Cu_2I_5$ MHPs were directly immersed in deionized water and ethanol, their blue PL intensity decreased to zero within minutes or hours, respectively. Although previous researches demonstrated that the process $Cs_3Cu_2I_5 \rightarrow CsCu_2I_3$ is reversible, orange emission belonging to $CsCu_2I_3$ was still observed when the polar solvent was removed. The inset of Figure 3b shows digital photographs of $Cs_3Cu_2I_5$ MHPs before and after treatment with polar solvents under excitation at 310 nm. The luminescence of the samples exhibits a blue coloration before treatment with polar solvents and transitions to an orange hue after treatment, indicating the formation of $CsCu_2I_3$ MHPs. This was also confirmed by the corresponding normalized PL spectra at 310nm excitation (Figure 3d). In addition, the XRD patterns also confirm the existence of the $CsCu_2I_3$ phase, and the ethanol-immersed powders with stronger orange PL intensity show stronger $CsCu_2I_3$ diffraction peak, as displayed in Figure S7 and S8.[27-28] In contrast, when $Cs_3Cu_2I_5$@Borosilicate is stored in deionized water and ethanol, its PL intensity is hardly reduced, as shown in Figure 3c and 3d. Figure 3e presents the experimental data on $Cs_3Cu_2I_5$@Borosilicate stability in deionized water, which always maintains bright blue luminescence. Similarly, when $Cs_3Cu_2I_5$ MHPs encounter dimethyl sulfoxide (DMSO), N, N-dimethylformamide (DMF) and methanol (MeOH), the corresponding PL intensity decreases to zero in minutes, as shown in Figure 3f. Notably, $Cs_3Cu_2I_5$@Borosilicate still has ultra-high stability and maintains high PL intensity in DMSO, DMF and MeOH for more than 10 days, as displayed in Figure 3g.

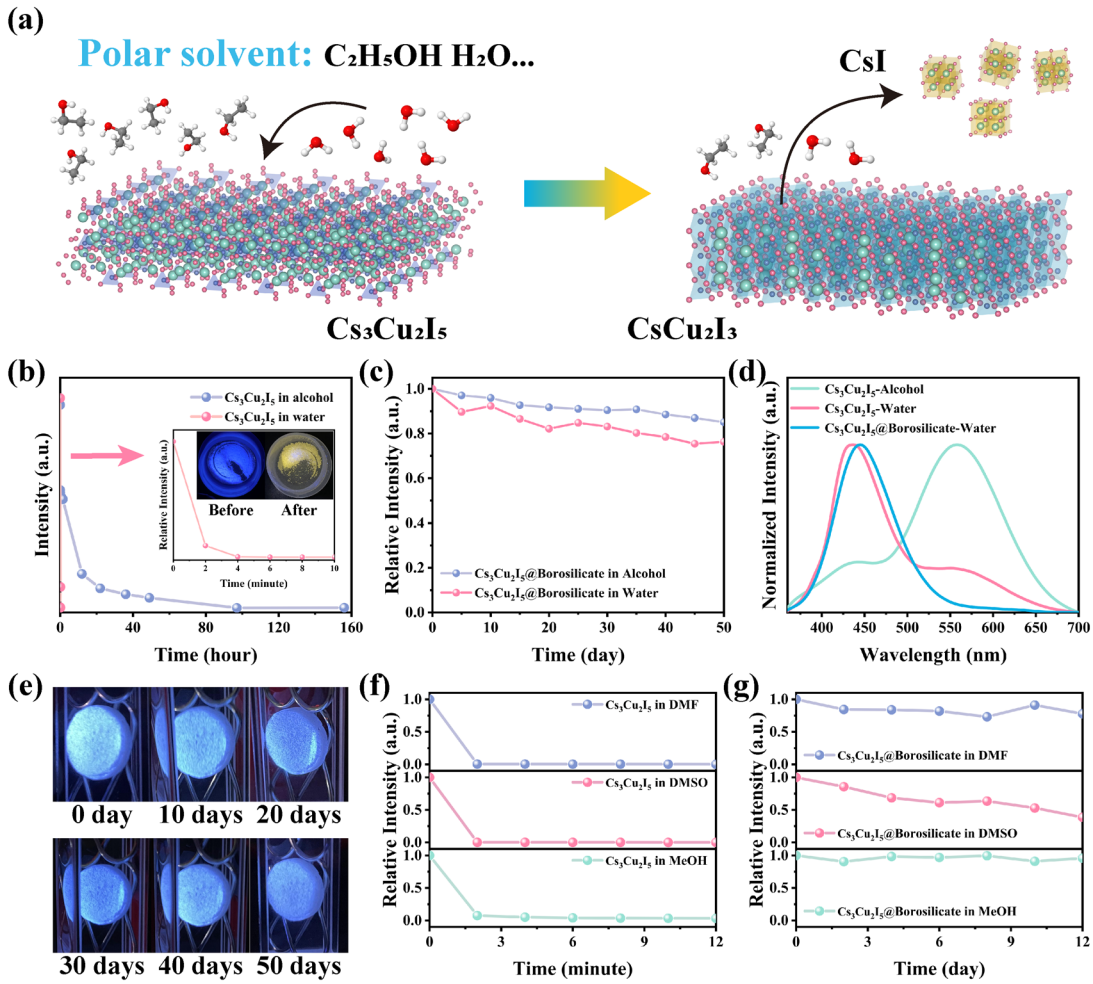


**Figure 3.** a) Schematic diagram of $Cs_3Cu_2I_5$ chemical decomposition process in polar solvent. Time-dependent PL intensity of b) $Cs_3Cu_2I_5$ MHPs and c) $Cs_3Cu_2I_5$@Borosilicate stored in deionized water and ethanol for different times, the inset presents digital photos of $Cs_3Cu_2I_5$ MHPs before and after exposure to polar solvents under excitation at 310 nm. d) The normalized PL spectra of $Cs_3Cu_2I_5$ MHPs and $Cs_3Cu_2I_5$@Borosilicate following dehydration and dealcoholization. e) The photograph of $Cs_3Cu_2I_5$@Borosilicate immersed in deionized water for different days. Time-dependent PL intensity of f) $Cs_3Cu_2I_5$ MHPs and g) $Cs_3Cu_2I_5$@Borosilicate stored in DMF, DMSO and MeOH for different time.

Moreover, the thermal stability of $Cs_3Cu_2I_5$ MHPs under different atmospheres was studied. The XRD pattern of the $Cs_3Cu_2I_5$ MHPs with heat-treatment at 643 K for 1 hour in air is shown in **Figure 4**a. It can be seen that the XRD pattern is mainly dominated by CsI, indicating that the structure of $Cs_3Cu_2I_5$ MHPs is destroyed. The XRD pattern of the $Cs_3Cu_2I_5$ MHPs with heat treatment at 643 K for 1 hour in a vacuum is shown in Figure 4b. Notably, the $Cs_3Cu_2I_5$ MHPs maintain their structure, which is further confirmed by the XRD refinement, as

shown in Figure S9. As mentioned above, since the PL spectra could also provide some useful information about the structural transformation of a luminescent material, the PL spectra of the $Cs_3Cu_2I_5$ MHPs after heat treatment in air and vacuum were investigated, as shown in Figure 4c. Compared with the PL intensity of $Cs_3Cu_2I_5$ MHPs heated in air, the PL intensity of $Cs_3Cu_2I_5$ MHPs heated in vacuum is significantly higher. In addition, the photographs of $Cs_3Cu_2I_5$ MHPs with heat treatment in air and vacuum under daylight and UV light are presented in the inset of Figure 4c. Specifically, air-heat-treated $Cs_3Cu_2I_5$ MHPs turn grey in daylight and have a much weaker PL intensity under UV light compared to vacuum-heat-treated $Cs_3Cu_2I_5$ MHPs. Moreover, the PL spectra of $Cs_3Cu_2I_5$ MHPs after heat treatment at different temperatures in air were studied, as shown in Figure S10. It is clear that the $Cs_3Cu_2I_5$ MHPs heated to higher temperatures show weaker PL intensity. According to our results, the thermal decomposition product of $Cs_3Cu_2I_5$ MHPs in air is only CsI without intermediate products $CsCu_2I_3$, which is different from the decomposition process of $Cs_3Cu_2I_5$ MHPs in polar solvent (Figure S7). Although the detailed reaction process is not clear yet, we speculate that $Cs_3Cu_2I_5$ MHPs are more likely to thermally decompose into CsI and CuI in the air, and then most of the CuI is volatilized and a small portion is oxidized to CuO,[29] changing the remaining powder from white to black, with a possible schematic depicted in Fig. 4d. Therefore, encapsulating may help to avoid the decomposition of $Cs_3Cu_2I_5$ MHPs.

To validate this conclusion, the temperature-dependent PL pseudocolor map of $Cs_3Cu_2I_5$ MHPs and $Cs_3Cu_2I_5$@Borosilicate were investigated, and the results were shown in Figure 4e and 4f, respectively. Figure 4g displays the plots of temperature-dependent (from 300K to 480K) PL relative intensity. The PL intensity of the $Cs_3Cu_2I_5$ MHPs decrease monotonically, indicating that lattice expansion and more phonons coupling with excitons occur at higher temperatures, leading to the activation of nonradiative recombination processes. Similarly, the $Cs_3Cu_2I_5$@Borosilicate composite also exhibits a monotonic downward trend in PL intensity. It is worth noting that at a temperature of 348 K, the PL intensity of the $Cs_3Cu_2I_5$@Borosilicate composite still has 56.7 % of the initial value, whereas the $Cs_3Cu_2I_5$ MHPs only has 43.2 % of the initial value, as shown in Figure 4g. This may be due to the tendency of decomposition of $Cs_3Cu_2I_5$MHPs at high temperatures in air. In contrast, the $Cs_3Cu_2I_5$@Borosilicate composite prevents air from penetrating the glass matrix, providing a vacuum-like condition for $Cs_3Cu_2I_5$ MHPs. Overall, these results indicate that encapsulating can avoid the decomposition of $Cs_3Cu_2I_5$ MHPs (Figure 4h), improve its stability, and verify the potential of the composite material in practical applications.

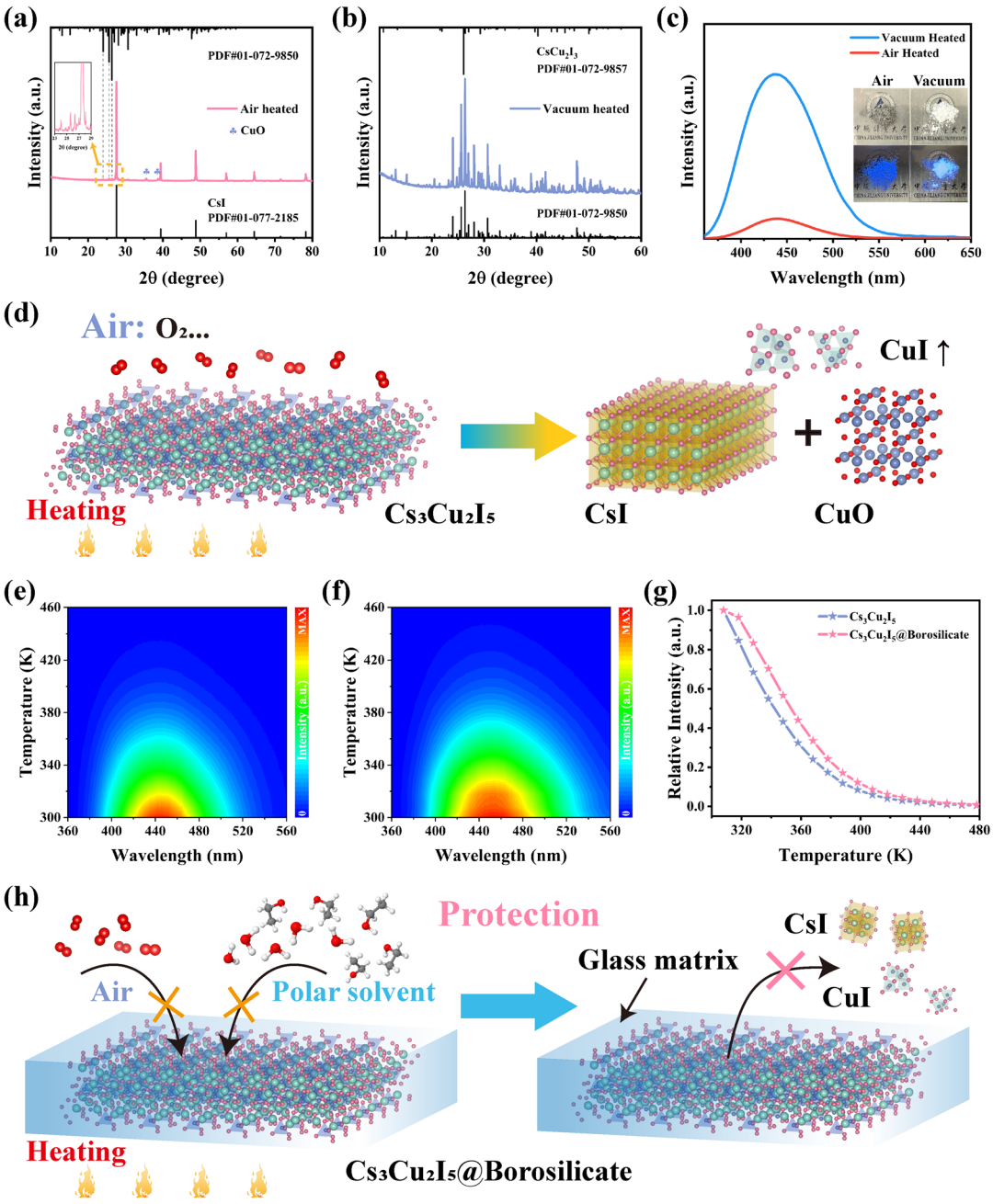


**Figure 4.** XRD patterns of $Cs_3Cu_2I_5$ MHPs after heating in different atmospheres: a) in air and b) in vacuum. c) PL spectra of the $Cs_3Cu_2I_5$ after heating to the melting point in different atmospheres, the inset presents its photograph under daylight (top) and 310 nm UV light (bottom). d) Schematic diagram of the $Cs_3Cu_2I_5$ chemical decomposition process in air. Pseudocolor map of temperature-dependent PL spectra of e) $Cs_3Cu_2I_5$ MHPs and f) $Cs_3Cu_2I_5$@Borosilicate. g) Temperature-dependent PL relative intensity of $Cs_3Cu_2I_5$ MHPs and $Cs_3Cu_2I_5$@Borosilicate. h) Schematic diagram of glass matrix protection $Cs_3Cu_2I_5$.

The high PLQY, broadband blue emission and zero self-absorption make the $Cs_3Cu_2I_5$ MHPs promising candidates for scintillators. Therefore, we analyzed the attenuation

coefficients of $Cs_3Cu_2I_5$, $CsPbBr_3$, CdTe, $Bi_4Ge_3O_{12}$ (BGO) and carbon dots over a broad range of photon energies, and the results are shown in **Figure 5**a. The results indicate that the attenuation coefficient of the $Cs_3Cu_2I_5$ perovskites across the entire energy region is close to that of CdTe and slightly lower than that of $CsPbBr_3$, which is proportional to the value of their $Z_{eff}$.[30] Figure 5b shows the radioluminescence (RL) spectrum of the $Cs_3Cu_2I_5$@Borosilicate composite measured at an X-ray source tube voltage of 50 kV, and the RL intensity increases with the increase of the $Cs_3Cu_2I_5$ MHPs concentration. Due to the lack of a self-absorption effect in $Cs_3Cu_2I_5$, the RL intensity is observed to incrementally rise with an increase in MHPs concentration up to 50 wt%, as illustrated in Figure S11. The digital photograph of the $Cs_3Cu_2I_5$@Borosilicate composite under X-ray excitation is depicted in the inset of Figure 5b. The decay kinetics under X-ray excitation of the $Cs_3Cu_2I_5$ perovskite and $Cs_3Cu_2I_5$@Borosilicate composites were profoundly investigated. The scintillation decay profiles of $Cs_3Cu_2I_5$@Borosilicate composite and $Cs_3Cu_2I_5$ MHPs were measured as shown in Figure 5c. The RL decay of $Cs_3Cu_2I_5$@Borosilicate and $Cs_3Cu_2I_5$ MHPs is well-fitted and suggested an average lifetime of 755 ns and 892 ns, respectively, which are in close proximity to the reported values.[31] The mechanism of RL in $Cs_3Cu_2I_5$ MHPs can be explained by the photoelectric ionization effect, as previously reported in halide perovskite scintillators.[6a] Similar to PL decay, the RL decay of the $Cs_3Cu_2I_5$@Borosilicate composite is shorter than that of $Cs_3Cu_2I_5$ MHPs. We speculate that it may be due to the bonding between a small part of $Cs_3Cu_2I_5$ and the borosilicate glass network, which leads to the change of Jahn-Teller distortion of the 0D electronic structure of $[Cu_2I_5]^{3-}$ octahedral, resulting in the change of scintillation decay.[32] $Cs_3Cu_2I_5$@Borosilicate composite and $Cs_3Cu_2I_5$ MHPs show the same radiation response, under a tube current range of 100-200 μA and a tube voltage of 50 kV, both the $Cs_3Cu_2I_5$ MHPs and $Cs_3Cu_2I_5$@Borosilicate composite displayed a linear response to the current (Figure 5d). The RL intensity of both $Cs_3Cu_2I_5$ MHPs and the $Cs_3Cu_2I_5$@Borosilicate composite shows a positive correlation with the applied voltages, over a range of 10-60 kV at a constant electron tube current of 200 μA, as illustrated in Figure S12. $Cs_3Cu_2I_5$@Borosilicate composite has a short RL decay time and linear response to the radiation can be used for rapid radiation detection.

To demonstrate the potential of $Cs_3Cu_2I_5$@Borosilicate scintillation material for X-ray imaging, a prototype projection system was established, as shown in Figure 5e, in which X-ray source, imaging object, $Cs_3Cu_2I_5$@Borosilicate composite and CMOS were sequentially placed. As shown in Figure 5f, the projection images of a chip and spring placed in the capsule were obtained by the current X-ray detection device. The projection system clearly reveals the

interior structure of the chip and capsule. To further evaluate X-ray imaging quality, we utilized the slanted-edge method to obtain the modulation transfer function (MTF) curve. The spatial frequency (lp $mm^{-1}$) at MTF = 0.2 is defined as the spatial resolution. The X-ray image for MTF calculation is shown in the inset of Figure 5g. As shown in Figure 5g, the image resolution with $Cs_3Cu_2I_5$@Borosilicate is ~7 lp $mm^{-1}$, which is superior to $CsPbBr_3$ quantum dots glass (4.1 lp $mm^{-1}$) [33] and traditional X-ray detector (CsI:Tl ~3 lp $mm^{-1}$, a-Se 4.75 lp $mm^{-1}$).[34] Notably, better image resolution can be obtained by reducing the refractive index difference between the $Cs_3Cu_2I_5$ MHPs and the glass matrix and improving the distribution of $Cs_3Cu_2I_5$ MHPs in the glass matrix. In addition, the RL intensity of the $Cs_3Cu_2I_5$@Borosilicate composite is stable under repeated X-ray irradiation with 10s on-off cycles (Figure 5h). It can be concluded that the $Cs_3Cu_2I_5$@Borosilicate composite exhibited excellent performance in X-ray imaging and long-term operational stability, and demonstrates great potential in medical diagnosis and industrial detection.

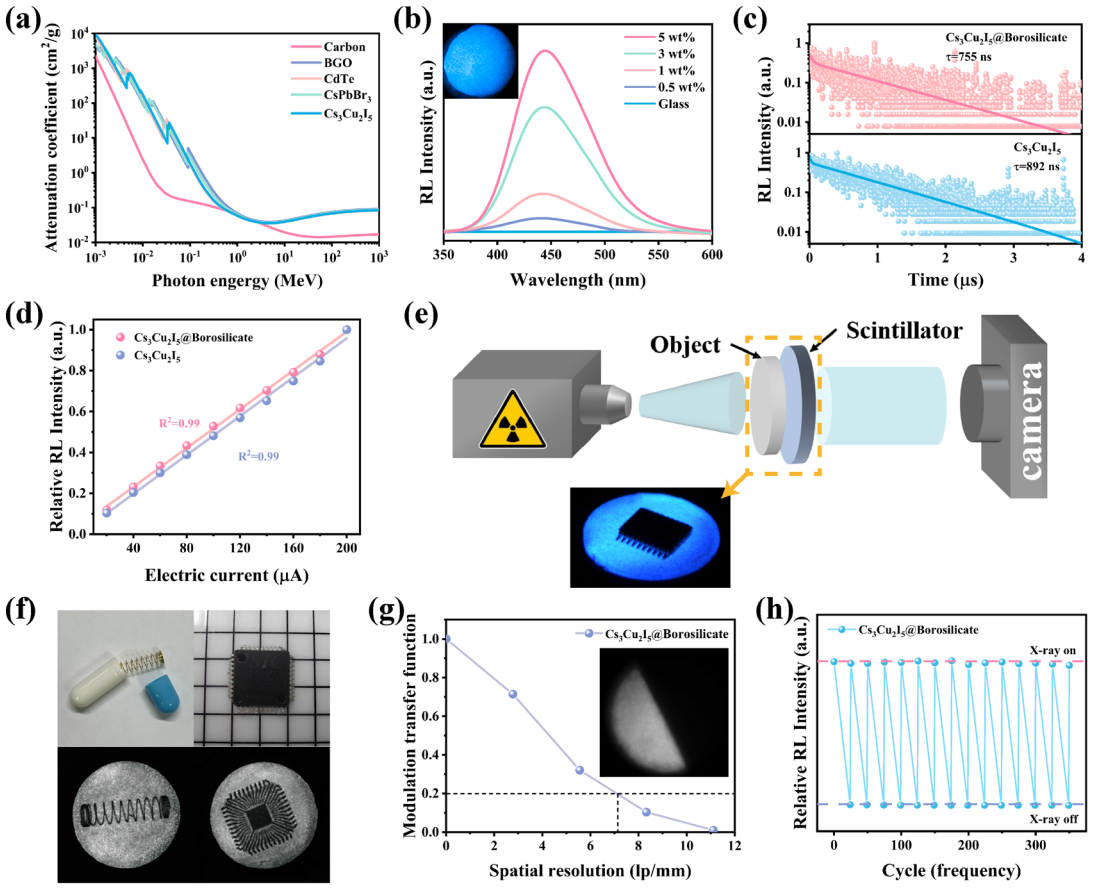


**Figure 5.** a) Attenuation coefficients of $Cs_3Cu_2I_5$, $CsPbBr_3$, CdTe, BGO and Carbon dots versus photons energy. b) The RL spectra of $Cs_3Cu_2I_5$@Borosilicate with different concentrations (tube voltage: 50 kV; tube current: 200 μA), the inset presents its photograph. c) Scintillation decay profiles of $Cs_3Cu_2I_5$@Borosilicate (top) and $Cs_3Cu_2I_5$ MHPs (bottom). d)

The response intensity of $Cs_3Cu_2I_5$ MHPs and $Cs_3Cu_2I_5$@Borosilicate as a function of electron tube current. e) Schematic of the prototype projection system for X-ray imaging, and the sequence is X-ray source, imaging object, $Cs_3Cu_2I_5$@Borosilicate composite and CMOS. f) The photograph and the corresponding X-ray image of a chip, spring placed in the capsule. g) MTF curves of X-ray images obtained from $Cs_3Cu_2I_5$@Borosilicate composite. h) The recorded RL intensity of $Cs_3Cu_2I_5$@Borosilicate under X-ray irradiation for repeated on-off cycles with a time interval of 10 s.

## 3. Conclusion

In summary, we report a rapid and facile approach for embedding MHPs into transparent inorganic glass matrix through SPS technology. This technique effectively preserved the exceptional optical properties of $Cs_3Cu_2I_5$ MHPs and enabled the successful preparation of $Cs_3Cu_2I_5$@Borosilicate composite. These composites exhibited intense blue light emission, a higher particle loading ratio, and excellent stability. The $Cs_3Cu_2I_5$@Borosilicate composite is significantly more resistant to polar solvents, extending durability from seconds or hours to months. In addition, these composites also exhibit superior thermal stability in air compared to $Cs_3Cu_2I_5$ MHPs. Furthermore, the capability of X-ray imaging was demonstrated through prototype experiments, which successfully obtained clear projection images of a chip and the internal spring of a capsule at an image resolution of approximately 7 lp $mm^{-1}$. Based on the aforementioned results, this novel composite, characterized by its exceptional optical and scintillation performance as well as its outstanding stability, is bound to create unlimited possibilities for optical devices that have been limited by existing approaches.

## 4. Experimental Section

### 4.1. Chemicals

Cesium iodide (CsI, 99.999%), Cuprous iodide (CuI, 99.95%) and dimethyl sulfoxide (DMSO, 99.8%) were purchased from Aladdin. Borosilicate glass powder (LX45) was purchased from Anywhere Powder company. Isopropanol (AR) was purchased from MACKLIN.

### 4.2. Synthesis of $Cs_3Cu_2I_5$ MHPs

CsI (1.2 mmol), CuI (0.8 mmol), and dimethyl sulfoxide (1.0 mL) were added to a small bottle (3 mL). The resulting mixture was heated to 333 K under vigorous stirring for 3 h, after which the powder was completely dissolved. Every 100 μL of the precursor was extracted into

3 mL of isopropanol and vibrated vigorously. $Cs_3Cu_2I_5$ MHPs were obtained by centrifugation at 10,000 rpm for 5 min and the supernatant was discarded. After the third centrifugation at 10,000 rpm for 5 min, the substrates were transferred to an oven and baked at 333 K until dryness.

### 4.3. Synthesis of $Cs_3Cu_2I_5$@Borosilicate by SPS technology

First, 0.05 g $Cs_3Cu_2I_5$ MHPs and 0.95 g borosilicate glass powder were uniformly mixed by mechanical milling. Then uniformly mixed composite powder loaded into the graphite die of 10 mm diameter using a sheet of flexible graphite sheet and carbon diffusion barrier to ensure the release of the solid and to protect the diffusion of the graphite component from the mold. The sintering process, as shown in Figure 1e, involved sintering at about 598 K under 18.7 MPa pressure for 3 min, which can obtain the best densification effect. Different concentrations were prepared following the same procedure.

### 4.4. Characterization Methods

The microstructure and chemical composition of the sample were analyzed by high-resolution transmission electron microscopy (HRTEM, FEI Tecnai G2F20 S-WTINE) and scanning electron microscopy (SEM, SU8010, Hitachi Ltd., Tokyo, Japan) coupled with an energy dispersive spectrometer (EDS). The crystal phases were examined by X-ray diffraction (XRD) with Cu Kα radiation (Rigaku SmartLab SE, Japan). The thermogravimetric analysis (TGA) and differential scanning calorimetry (DSC) scans were performed using NETZSCH STA 449F3 at a heating rate of 10 K $min^{-1}$. Steady-state PL spectra were obtained by using an Edinburgh Instruments (FLS1000) spectrometer. Time-resolved PL spectra were measured by the time-correlated single-photon counting method with an Edinburgh Instruments FLS1000 spectrometer after excitation with a 280 nm pulsed diode laser. Cathodoluminescence (CL) measurements were performed using a field emission scanning electron microscope (SEM) equipped with a CL system by SEM-CL Goldenscope Rainbow (CL-SEM, Gatan Mono CL4). In-situ X-ray diffraction (XRD) measurements were performed in air and vacuum, respectively, heated to 643K at a heating rate of 10 K $min^{-1}$ and recorded every 20 K (PANalytical Empyrean, Netherlands). The X-ray photoelectron spectroscopy (XPS) spectra were obtained using Thermo Scientific K-Alpha. The RL spectra were measured by a grating spectrometer (Omni-λ300i, Zolix, China). The scintillation decay curves were determined by an oscillograph (Tektronix DPO 5140). The tested samples were irradiated with 662 keV γ-rays from a $^{137}Cs$ source, and their scintillation photons were detected with the PMT (Hamamatsu R2059).

### 4.5. X-ray imaging experimental device system

In a typical procedure for X-ray imaging, The X-ray source (Pmax = 12 W, Vmax = 60 kV, Imax = 200 μA) was a miniature x-ray tube produced by Amptek company, which was vertically placed on the measured object and the film. The light path was finally collected by the CMOS with high sensitivity (Photometrics, Prime 95B).


### Acknowledgements

The authors sincerely acknowledge Prof. Yang (Michael) Yang for providing technology supporting in X-ray imaging.

This research was supported by National Natural Science Foundation of China (62205321); The Fundamental Research Funds for the Provincial Universities of Zhejiang (2022YW32); Natural Science Foundation of Zhejiang Province (Q21F050026);

Panyi Wang and Mengmeng Meng contribute equally.


### Conflict of Interest

The authors declare no conflict of interest.

### Data Availability Statement

Research data are not shared.

## References


[1] Z.-K. Tan, R. S. Moghaddam, M. L. Lai, P. Docampo, R. Higler, F. Deschler, M. Price, A. Sadhanala, L. M. Pazos, D. Credgington, Nat. Nanotechnol. **2014**, 9, 687.

[2] J.-P. Correa-Baena, M. Saliba, T. Buonassisi, M. Grätzel, A. Abate, W. Tress, A. Hagfeldt, Science **2017**, 358, 739.

[3] S. A. Veldhuis, P. P. Boix, N. Yantara, M. Li, T. C. Sum, N. Mathews, S. G. Mhaisalkar, Adv. Mater. **2016**, 28, 6804.

[4] X. Wang, Y. Wang, W. Gao, L. Song, C. Ran, Y. Chen, W. Huang, Adv. Mater. **2021**, 33, 2003615.

[5] a)X. Zhao, J. D. A. Ng, R. H. Friend, Z.-K. Tan, Acs Photonics **2018**, 5, 3866; b)Y. Dong, Y.-K. Wang, F. Yuan, A. Johnston, Y. Liu, D. Ma, M.-J. Choi, B. Chen, M. Chekini, S.-W. Baek, Nat. Nanotechnol. **2020**, 15, 668; c)L. Protesescu, S. Yakunin, M. I. Bodnarchuk, F.

Krieg, R. Caputo, C. H. Hendon, R. X. Yang, A. Walsh, M. V. Kovalenko, Nano Lett. **2015**, 15, 3692.

[6] a)Q. Chen, J. Wu, X. Ou, B. Huang, J. Almutlaq, A. A. Zhumekenov, X. Guan, S. Han, L. Liang, Z. Yi, Nature **2018**, 561, 88; b)J. H. Heo, D. H. Shin, J. K. Park, D. H. Kim, S. J. Lee, S. H. Im, Adv. Mater. **2018**, 30, 1801743; c)L. Wang, K. Fu, R. Sun, H. Lian, X. Hu, Y. Zhang, Nanomicro Lett. **2019**, 11, 1; d)Y. Zhang, R. Sun, X. Ou, K. Fu, Q. Chen, Y. Ding, L.-J. Xu, L. Liu, Y. Han, A. V. Malko, ACS Nano **2019**, 13, 2520; e)Y. Zhou, X. Wang, T. He, H. Yang, C. Yang, B. Shao, L. Gutiérrez-Arzaluz, O. M. Bakr, Y. Zhang, O. F. Mohammed, ACS Energy Lett. **2022**, 7, 844.

[7] T. Jun, K. Sim, S. Iimura, M. Sasase, H. Kamioka, J. Kim, H. Hosono, Adv. Mater. **2018**, 30, 1804547.

[8] L. Lian, M. Zheng, W. Zhang, L. Yin, X. Du, P. Zhang, X. Zhang, J. Gao, D. Zhang, L. Gao, Adv. Sci. **2020**, 7, 2000195.

[9] X. Zhao, T. Jin, W. Gao, G. Niu, J. Zhu, B. Song, J. Luo, W. Pan, H. Wu, M. Zhang, Adv. Opt. Mater. **2021**, 9, 2101194.

[10] X. Li, J. Chen, D. Yang, X. Chen, D. Geng, L. Jiang, Y. Wu, C. Meng, H. Zeng, Nat. Commun. **2021**, 12, 3879.

[11] a)Y. Zhou, Y. Zhao, Energy Environ. Sci. **2019**, 12, 1495; b)Y. Wei, Z. Cheng, J. Lin, Chem. Soc. Rev. **2019**, 48, 310.

[12] a)Y. Le, X. Huang, H. Zhang, Z. Zhou, D. Yang, B. Yin, X. Liu, Z. Xia, J. Qiu, Z. Yang, Adv. Photonics **2023**, 5, 046002; b)J. Lin, Y. Lu, X. Li, F. Huang, C. Yang, M. Liu, N. Jiang, D. Chen, ACS Energy Lett. **2021**, 6, 519; c)S. Yuan, D. Chen, X. Li, J. Zhong, X. Xu, ACS Appl. Mater. Interfaces **2018**, 10, 18918.

[13] M. Xia, J. Luo, C. Chen, H. Liu, J. Tang, Adv. Opt. Mater. **2019**, 7, 1900851.

[14] Q. Pan, D. Yang, G. Dong, J. Qiu, Z. Yang, Prog. Mater Sci. **2022**, 130, 100998.

[15] a)W. Lv, L. Li, M. Xu, J. Hong, X. Tang, L. Xu, Y. Wu, R. Zhu, R. Chen, W. Huang, Adv. Mater. **2019**, 31, 1900682; b)X. Liu, W. Xie, Y. Lu, X. Wang, S. Xu, J. Zhang, J. Mater. Chem. C **2022**, 10, 762.

[16] Q. Yang, H. Wei, G. Li, S. Zhao, Y. Ao, X. Liu, L. Fu, G. Cai, Chem. Eng. J. **2024**, 483, 149288.

[17] M. Meng, P. Wang, Y. Yuan, M. Cai, L. Calvez, J. Rocherulle, H. Ma, J. Zhang, S. Xu, X. Zhang, Ceram. Int. **2023**, 49, 10181.

[18] C. Yang, B. Zhuang, J. Lin, S. Wang, M. Liu, N. Jiang, D. Chen, Chem. Eng. J. **2020**, 398, 125616.

[19] W. Cui, J. Zhao, L. Wang, P. Lv, X. Li, Z. Yin, C. Yang, A. Tang, J. Phys. Chem. Lett. **2022**, 13, 4856.

[20] A. Wojakowska, A. Górniak, A. Y. Kuznetsov, A. Wojakowski, J. Josiak, J. Chem. Eng. Data **2003**, 48, 468.

[21] a)N. H. Perry, S. R. Bishop, H. L. Tuller, J. Mater. Chem. A **2014**, 2, 18906; b)Q. Jiang, M. Chen, J. Li, M. Wang, X. Zeng, T. Besara, J. Lu, Y. Xin, X. Shan, B. Pan, ACS Nano **2017**, 11, 1073.

[22] M. Cai, L. Calvez, J. Rocherulle, P.-A. Bouit, M. Hissler, H. Ma, C. Roiland, V. Dorcet, J. Zhang, S. Xu, J. Alloys Compd. **2022**, 897, 163196.

[23] a)H. Lin, C. Zhou, Y. Tian, T. Siegrist, B. Ma, ACS Energy Lett. **2017**, 3, 54; b)C. Zhou, H. Lin, Y. Tian, Z. Yuan, R. Clark, B. Chen, L. J. van de Burgt, J. C. Wang, Y. Zhou, K. Hanson, Chem. Sci. **2018**, 9, 586; c)C. Zhou, H. Lin, H. Shi, Y. Tian, C. Pak, M. Shatruk, Y. Zhou, P. Djurovich, M. H. Du, B. Ma, Angew. Chem. Int. Ed. **2018**, 130, 1033; d)Q. He, C. Zhou, L. Xu, S. Lee, X. Lin, J. Neu, M. Worku, M. Chaaban, B. Ma, ACS Mater. Lett. **2020**, 2, 633.

[24] a)T. Hu, M. D. Smith, E. R. Dohner, M.-J. Sher, X. Wu, M. T. Trinh, A. Fisher, J. Corbett, X.-Y. Zhu, H. I. Karunadasa, J. Phys. Chem. Lett. **2016**, 7, 2258; b)C. Zhou, H. Lin, M. Worku, J. Neu, Y. Zhou, Y. Tian, S. Lee, P. Djurovich, T. Siegrist, B. Ma, J. Am. Chem. Soc. **2018**, 140, 13181.

[25] G. Hou, C. Zhang, W. Fu, G. Li, J. Xia, Y. Ping, J. Lumin. **2020**, 217, 116769.

[26] Z. Ma, X. Ji, S. Lin, X. Chen, D. Wu, X. Li, Y. Zhang, C. Shan, Z. Shi, X. Fang, Adv. Mater. **2023**, 35, 2300731.

[27] J. Feng, J. Wang, D. Wang, M. Han, G. Qian, F. Wu, Q. Lin, Z. Hu, ACS Appl. Electron. Mater. **2022**, 4, 225.

[28] D. Lee, S. J. Lee, J. H. Kim, J. Park, Y. C. Kang, M. Song, H. W. Lee, H. S. Kim, J. W. Choi, Adv. Funct. Mater. **2022**, 32, 2202207.

[29] P. Darnige, Y. Thimont, L. Presmanes, A. Barnabé, J. Mater. Chem. C **2023**, 11, 630.

[30] B. Yang, L. Yin, G. Niu, J. H. Yuan, K. H. Xue, Z. Tan, X. S. Miao, M. Niu, X. Du, H. Song, Adv. Mater. **2019**, 31, 1904711.

[31] Q. Wang, Q. Zhou, M. Nikl, J. Xiao, R. Kucerkova, A. Beitlerova, V. Babin, P. Prusa, V. Linhart, J. Wang, Adv. Opt. Mater. **2022**, 10, 2200304.

[32] a)B. M. Benin, D. N. Dirin, V. Morad, M. Wörle, S. Yakunin, G. Rainò, O. Nazarenko, M. Fischer, I. Infante, M. V. Kovalenko, Angew. Chem. Int. Ed. **2018**, 57, 11329; b)H. Yin, X. Zhang, L. Li, Z. Zhang, X. Gong, R. Ding, C. Li, Y. Zhang, ACS Appl. Mater. Interfaces **2021**, 13, 30008; c)Y. Hui, S. Chen, R. Lin, W. Zheng, F. Huang, Mater. Chem. Front. **2021**, 5, 7088;

d)J. Liu, X. Zhao, Y. Xu, H. Wu, X. Xu, P. Lu, X. Zhang, X. Zhao, M. Xia, J. Tang, Laser Photonics Rev. **2023**, 17, 2300006.

[33] W. Ma, T. Jiang, Z. Yang, H. Zhang, Y. Su, Z. Chen, X. Chen, Y. Ma, W. Zhu, X. Yu, Adv. Sci. **2021**, 8, 2003728.

[34] P. Büchele, M. Richter, S. F. Tedde, G. J. Matt, G. N. Ankah, R. Fischer, M. Biele, W. Metzger, S. Lilliu, O. Bikondoa, Nat. Photonics **2015**, 9, 843.